

## FLOW INSTABILITY OF DOPE SOLUTION IN HOLLOW FIBER SPINNING PROCESS FOR DIFFERENT FLOW CHANNEL LENGTH

\*Mohd Suffian M., Rosalam S., Mohd Azlan I., Chua B. L., & Santha Pang H. Y.

School of Engineering and Information Technology  
Universiti Malaysia Sabah, Jalan UMS, 88450 Kota Kinabalu, Sabah, Malaysia

**ABSTRACT.** *The study demonstrated the effect of different flow channel length on the spinneret with respect to the ceramic hollow fiber membrane morphology. A smartly designed spinneret is utilized for the spinning process where the nozzle used can be change to different length via the use of adapters. Thus, allowing the effect of having different flow channel length to be investigated. Three spinneret adapters with different nozzle length were fabricated at 29 mm, 34 mm, and 39 mm. Ceramic hollow fiber membrane is produced using these configurations in the spinning process. Then, the micrographic cross sections of hollow fiber membranes is investigated using Scanning Electron Microscope (SEM) where it shows finger like, dense layer and damage structure morphology. Out of the samples investigated, hollow fiber membrane spun using 39 mm nozzle length produce the best concentricity. CFD simulation is initiated to study the flow behavior inside the flow channel to correlate with that of the experimental result attained.*

**KEYWORDS.** Hollow fiber, Spinneret, Flow Channel, CFD

### INTRODUCTION

Over the decades, membrane filtration has become firmly established as the primary technology for ensuring the purity, safety or efficiency of the treatment of water or effluents. It has played an important role in large areas of expertise ranging from water treatment to industrial gas separation and purification which proves critical in today's global crisis. Applications include, the desalination of seawater by reverse osmosis to provide drinking quality water, hemodialysis, and water and nitrogen recovery from air using gas separation method (Su, 2007). The chemical industry in particular is a growing field in the application of membranes, which, however, often requires membrane materials with exceptional stability, efficient and of high quality variants.

In general, membrane can be described as a perm-selective barrier or a fine sieve, which under the effect of a transfer force, will allow or prohibit the passage of certain components between two separate mediums. They are normally further classified according to their morphology such as dense, porous and composite. Permeability and separation factor of a membrane is the two most important performance indicators, which normally govern by thickness, pore size and surface porosity of the said membrane. Most of the presently available membranes are porous or consist of a dense top layer on a porous structure (Nunes and Peineman, 2006). Hollow fiber membrane has gained popularity over the years due to its high surface area to volume ratio, which provides the ability to achieve a given separation while occupying a much smaller space.

Spinning technique used in fabrication of hollow fiber membrane is a complex process and requires tight quality control; this is caused by the viscous solution extruded from a complicated channel within a tube-orifice spinneret. Some factors affecting the hollow fiber membrane formation are identical with other configuration such as; polymer content, additives in coagulating fluid and temperature of the coagulant. However, there are other

variables unique to the hollow fiber spinning process, which affects the fiber morphology such as; (a) Velocity of the spinning solution (b) Velocity of coagulating fluid (c) Distance of “air gap” between spinneret and the collecting bath (Porter, 1990). One of the observed characteristics in the spinning process is the spinning stability and the distortion mechanism. The proposed mechanisms of extrudate distortion implicate one or more of the following parameters (Petrie and Denn, 1976): (1) fracture; (2) Reynolds turbulence; (3) thermal effects; (4) die entry and exit effects; (5) rheological effects; and (6) slip at the die wall. As a rule of thumb, most researchers agreed that the distortions of polymer extrudate most likely appear when the recoverable shear, which is defined as the ratio of the die wall shear stress to the elastic shear modulus, reaches a critical value of 1–10 (Larson, 1992; Petrie and Denn, 1976). Therefore, any efforts to reduce or completely eliminate the distortions in the polymer flow must take into consideration some major parameters when spinning hollow fibers from a polymer solution, which is: (1) spinneret designs; (2) dope solution flow rate and rheology; (3) spinning temperature; (4) air gap distance; and (5) take-up speed. Although the extrudate flow behavior was not governed only by technical parameters as it is also influenced by the material characteristic used as demonstrated by Piau *et al.* (1988), Yang *et al.* (2008), and den Otter (1971). This manuscript, however, will only concentrate on spinneret design at constant spinning parameters only.

Shear stress is developed when a fluid is in motion. When a viscous polymer solution is extruded through the small size annulus of a spinneret, it will subject to shear stress even though the traversing time of a polymeric dope solution is normally short as it involves only a few millimeters in the annulus. Other researchers have investigated and ascertained that the presence of flow induces shear stress affect the rheological behavior to a certain degree (Wang *et al.*, 2004; Chung *et al.*, 2001; Qin *et al.*, 2001; Chung *et al.*, 1998). The particles of the fluid move relative to each other in a typical spinneret so that they have different velocities, causing the original shape of the fluid become distorted (John, 2001). The dope solution itself does not follow typical Newtonian fluid behavior (Bird *et al.*, 1987) further complicates the flow mechanism inside the spinneret. Therefore, it is vital to study the fluid behavior and its correlation with spun hollow fibers characteristic.

To produce the hollow fiber membrane economically, one would need an efficient spinning system where the fiber production rate is maximized while maintaining low cost. However, as mentioned before the spinning process is very delicate and governs by several factors. Incorrect spinning parameters can lead to undesirable characteristic such as sharkskin, un-axisymmetric structure and other instability related problem increasing the cost of producing the membrane. Researchers (Larson, 1992; Petrie and Denn, 1976; Piau *et al.*, 1990; Moynihan *et al.*, 1990; Santoso, 2006; Bonyadi and Chung, 2007; Nijdam *et al.*, 2005) have been long studying the issues encompassed within the fiber spinning instability which include: (1) draw resonance; (2) necking; (3) capillary break-up; irregular cross-section and (5) melt fracture or extrudate distortion (Widjojo and Chung, 2006). The instability phenomena lead to fiber breakage during the spinning process, generate a non-uniform cross-sectional diameter along the spun fibers and distorted gross or wavy polymer flow.

This manuscript focuses on the effect of having different flow channel length to ceramic hollow fiber membrane morphology. Furthermore, the velocity behavior inside the dope flow channel for different length is simulated. In this regard, the objectives are; (1) To investigate and compare the effect of different flow channel to the hollow fiber membrane morphology, (2) To come out with a suggestion on how to improve hollow fiber morphology.

## EXPERIMENTAL

### *Materials*

Kaolin powders, polyethersulfone (PESF) in pellet form and N-methyl-2-pyrrolidone (NMP, 99% extra pure) were purchased from Sigma Aldrich; each was used as an additive and solvent. Each material was prepared and weighted according to the amount as shown in Table 1. The suspensions are prepared and mixed in a laboratory blue cap bottle 250 ml on a hot plate stirrer (Lab Depot, Inc). PESF is added slowly to NMP solution while the hot plate stirrer is switched on at a constant speed and temperature of 60°C. Once the PESF is fully dissolved, Kaolin powder was slowly added to the solution. Finally, the Kaolin suspension was put on a roller machine for 48 hours to ensure homogenous mixture.

Prior to the spinning process, viscosity of the kaolin suspension was measured using a rotational viscometer Brookfield's Programmable HADV-IV + Rheometer. The viscosity of the kaolin suspension is determined from the measured torque necessary to overcome the viscous resistance when spindle no. 5 rotates in the sample container. The viscosity corresponding to the kaolin content at spinning temperature of 25°C was obtained and listed in Table 1.

**Table 1. Kaolin Suspension material Properties.**

<b>Spinning Parameter</b>	<b>Condition</b>
Dope Composition (g)	27/150.75/54 (PES/NMP/Kaolin)
Dope Composition (wt%)	11/65/24(PES/NMP/Kaolin)
Dope Viscosity (cp)	$7.3 \times 10^3$
Dope Density (g/ml)	0.55236

### *Spinning Process of Hollow Fiber Membrane and Scanning Electron Microscope (SEM) Observation*

Asymmetric hollow fiber membranes were fabricated through dry-wet spinning process with force convection in the dry gap (Li, 2007). The synthesized dope solution was transferred into a stainless steel dope reservoir, from which dope was fed into the annulus of the spinneret under pressurized nitrogen gas. The nitrogen and bore fluid was set to desired pressure and flow rate, respectively. A 50-liter coagulation bath was initially prepared prior of the spinning process. The bore fluid was let to flow prior the dope extrusion, and then gas control valve was opened slowly to control the dope flow. Tap water at 25 °C was used as the external coagulant agent in the coagulation bath. The spun fibers were rinsed with water at room temperature for at least 24 hour to remove the residue NMP. The process is then repeated for each different nozzle length and the coagulant (water) was renewed for each spinning process. Detail spinning condition is as shown in Table 2.

**Table 2. Experiment Parameter of spinning hollow fiber membrane.**

<b>Spinning Parameter</b>	<b>Condition</b>
<b>Dope Flow rate (bar)</b>	2 (pressure regulated)
<b>Bore fluid</b>	Treated tap water
<b>Bore fluid flow rate (ml/s)</b>	1 (as indicated by gear pump)
<b>Air gap length (cm)</b>	3
<b>Spinning temperature (<sup>0</sup>C)</b>	28
<b>Humidity (%)</b>	60
<b>Take-up speed</b>	Free fall
<b>Spinneret Geometry</b>	
<b>i. Nozzle ID (mm)</b>	1.8
<b>ii. Needle OD (mm)</b>	1.6
<b>iii. Needle ID (mm)</b>	1.2
<b>iv. Needle Length (mm)</b>	29/34/39

To observe the hollow fiber morphology under Scanning Electron Microscope (SEM), the spun hollow fiber needs to be prepared first. The preparation procedures are as follow; the fibers are first dried to ensure that liquid are removed from the specimen to prevent vaporization during observation with SEM. Then, it is quenched in a liquid nitrogen solution, which brought the specimen to cryogenic state. Next, a thin layer of Joel JFC-11-E is sputtered on the fiber membrane using a sputting device. Finally, images of the hollow fiber membrane were taken at magnification size 31 (combination 2) and 34 (combination 3) respectively.

**Spinneret Design and Construction**

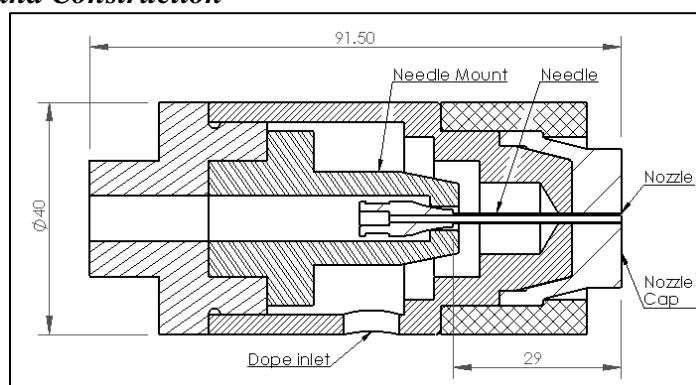
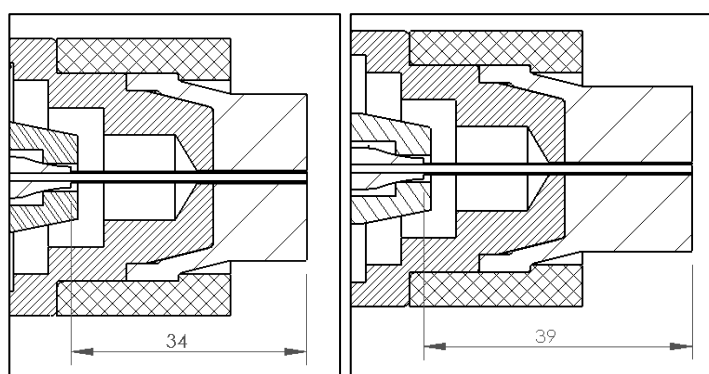


**Figure 1. Spinneret with Needle Length 29 mm.**



**(a) Needle length 34 mm                      (b) Needle length 39 mm**

**Figure 2. Spinneret Needle Length.**

A spinneret as shown in Figure 1 and 2 was used to investigate the flow channel behavior with respect to the length. Three nozzles as shown in figure 3 (a) were used which are compatible with the spinneret; the nozzles are in 29 mm, 34 mm, and 39 mm length. The difference of each channel length translates to different traversing (residence) time of the dope solution, where shorter nozzle having shortest time and vice versa. Three matting cap nozzle were fabricated to accommodate the different size nozzle using an in-house lathe machine. Each spinneret caps have the flow channel of 4 mm, 9 mm, and 14 mm as shown in Figure 3 (b).



**Figure 3. (a) Nozzle Length in 29 mm, 34 mm, and 39 mm; (b) Cap Nozzle**

#### ***Computational Fluid Dynamic (CFD) Simulation and Assumption***

The CFD simulation was carried out using *Solidworks Flowworks* software to simulate the dope solution flow through the spinneret. CFD with *Flowworks* is a typical process and can be underline in the following steps;

- (a) Modeling of the spinneret in *solidworks*.
- (b) Designation of the computational domain and mesh properties.
- (c) Boundary condition, material parameter and goal insertion.
- (d) Result interpretation.

In simulating the dope solution flow, isothermal melt spinning is considered. Thus, energy and mass transfer is not solved in the simulation work. This simulation is only governed by the continuity and momentum conservation equations. Other assumptions were made, mainly;

- a) The spinning process are in steady state
- b) Fully develop flow at the inlet of the spinneret.
- c) Homogeneous suspension.
- d) Gravity effect and friction due to surface roughness are negligible.
- e) The solution is incompressible Newtonian fluid.

Su *et. al* (2006) argues that the assumption of a Newtonian clad fluid to be valid for sufficiently low die shear rates, it will also provide a good basis for interpreting non-Newtonian effects in future works. Similar approach was taken by Widjojo *et al.* (2010) in simulating the dope solution flow characteristic. The boundary conditions in the computational domain were set as follow;

- a) Inlet pressure at 2 bar
- b) Outlet pressure at atmospheric pressure and
- c) No slip condition inside the spinneret wall.

The simulation is considered to reach steady state if there is no significance change in pressure and velocity detected. To do this, global pressure and velocity goal as the convergence criteria were set before the simulation process started. Simulation is completed if both goals were reached.

## RESULT AND DISCUSSION

### *The Effect of Flow Channel Length on Hollow Fiber Membrane Spinning*

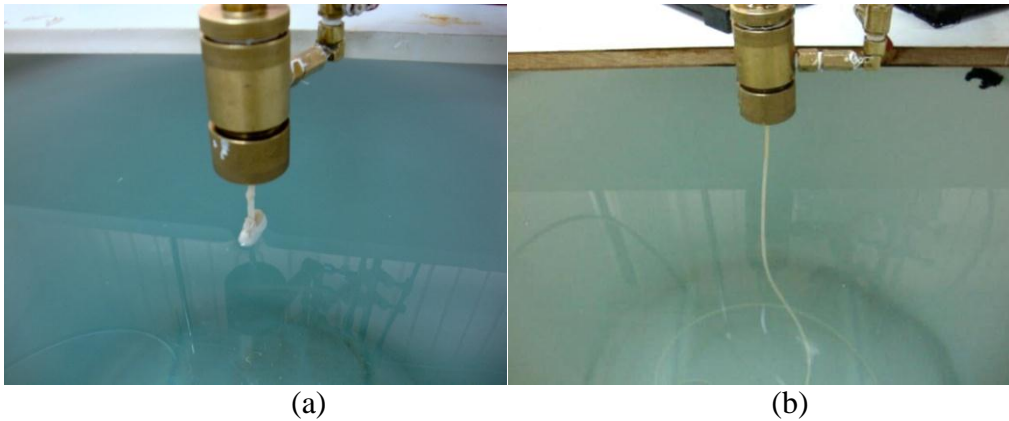


**Figure 4. (a) Agglomeration; (b) Smooth Spinning**

Hollow fiber spinning using 29 mm nozzle was not successful; this was caused by agglomeration that took place as shown in Figure 4 (a). To understand the cause of the agglomeration, one needs to understand the die swell formation theory. The die swell formation is influenced by the material characteristic itself and the different spinneret geometry design that employed. At the exit of the channel, die swell is formed due to the memory effect exhibited by a non-Newtonian polymeric fluid (Widjojo *et al.*, 2010). If a stable die swell fails to establish itself during the spinning process, coupled with chain relaxation and the unsteady state flow; the flow instability in the die swell area causes it to collapse and agglomerates at the exit of the spinneret as encountered in the experiment.

On the other hand, fiber spinning process for nozzle length 34 mm and 39 mm proceed smoothly. There was no significant difference observed during the spinning process as shown in Figure 5 (b). However, perfect concentric hollow fiber membrane was not achieved in any of the configuration as shown by the SEM figures in the next section.

### ***Hollow Fiber Morphology***

In order to observe the hollow fiber morphology especially its structure and concentricity, the hollow fiber specimens were observed under SEM.

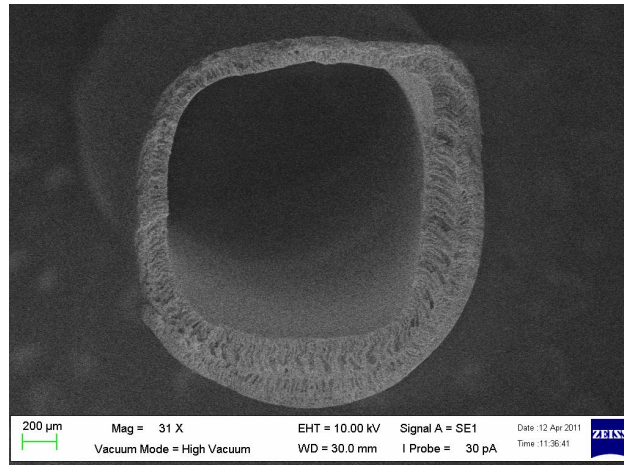


**Figure 6. Morphology of Hollow Fiber Membrane at 31x (Nozzle - 39 mm).**

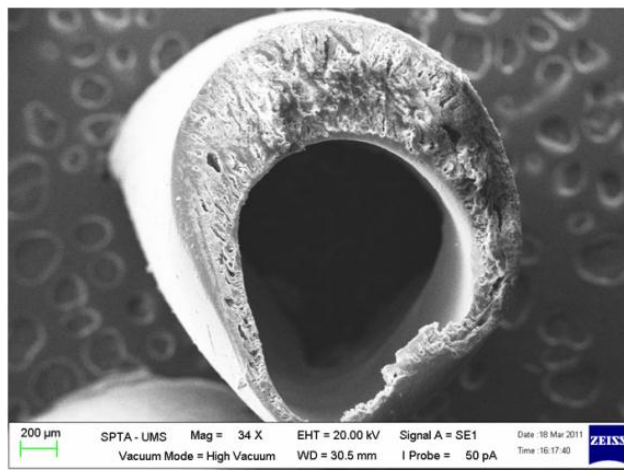


**Figure 7. Morphology of Hollow Fiber Membrane at 34x (Nozzle – 34 mm).**

From the Figure 6 and Figure 7, it is clearly shown that the hollow fiber membranes are asymmetric, exhibiting finger like dense layer typical of a hollow fiber membrane. However, the thickness of the membrane appears uneven and shows visible structural damage for both configurations. Comparisons of SEM figures between configurations show that combination 3 exhibits better concentricity level and structural integrity compared to combination 2. Since flow behavior inside the spinneret is difficult to analyze due to the extreme small size of the annulus (at 1.8 mm); simulation result is interpreted and visualize instead in an effort to understand and to correlate with experimental data.

**Flow Velocity Gradient at Point of Interest**

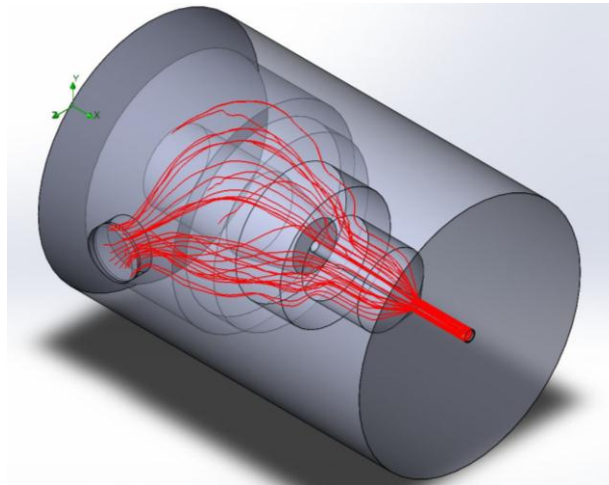


**Figure8. Simulated Velocity Trajectories.**

The simulated velocity trajectory as shown in Figure 8 indicates two points of interest inside the spinneret; a) Annulus inlet and, b) Annulus outlet. Observation of the annulus inlets shows that the velocity trajectory entering the annulus is not symmetric due to suspension inlet location; thus forcing the solution to travel at different route as demonstrated in Figure 9. This affects suspension velocity gradient entering the annulus as well as inside the annulus channel. The exit point of the solution is also observed because the variance of velocity at this point will affect the concentricity of the spun hollow fiber membrane. To observe the velocity gradient at the said location, cut plot were made at plane Y-X and plane Z-X. To identify the cut plots better, quadrants were designated to the cut plot as shown in Table 3. Table 4 shows the velocity gradients of each combination for comparison purpose.

**Table 3. Quadrant Identity.**

Quadrant Identifier	Plane	Cut Plot (Configuration 1 : 29 mm)
	Y-X	
	Z-X	



**Table 4. Velocity Gradient at Annulus.**

Plane	Velocity Gradient	Scale
<b>Configuration 1 : 29 mm</b>		
Y-X		<ul style="list-style-type: none"> <li>0.004</li> <li>0.004</li> <li>0.004</li> <li>0.003</li> <li>0.003</li> <li>0.002</li> <li>0.002</li> <li>0.002</li> <li>0.001</li> <li>0.001</li> <li>6.848e-04</li> <li>3.424e-04</li> <li>3.617e-09</li> </ul> Velocity [m/s]
Z-X		<ul style="list-style-type: none"> <li>0.003</li> <li>0.003</li> <li>0.003</li> <li>0.002</li> <li>0.002</li> <li>0.002</li> <li>0.001</li> <li>0.001</li> <li>9.912e-04</li> <li>7.434e-04</li> <li>4.956e-04</li> <li>2.478e-04</li> <li>3.617e-09</li> </ul> Velocity [m/s]
<b>Configuration 2 : 34 mm</b>		
Y-X		<ul style="list-style-type: none"> <li>0.003</li> <li>0.003</li> <li>0.003</li> <li>0.002</li> <li>0.002</li> <li>0.002</li> <li>0.001</li> <li>0.001</li> <li>8.394e-04</li> <li>6.715e-04</li> <li>5.036e-04</li> <li>3.356e-04</li> <li>1.679e-04</li> <li>2.183e-08</li> </ul> Velocity [m/s]
Z-X		<ul style="list-style-type: none"> <li>0.002</li> <li>0.002</li> <li>0.002</li> <li>0.002</li> <li>0.002</li> <li>0.001</li> <li>0.001</li> <li>9.289e-04</li> <li>7.862e-04</li> <li>6.635e-04</li> <li>5.308e-04</li> <li>3.981e-04</li> <li>2.654e-04</li> <li>1.327e-04</li> <li>2.205e-09</li> </ul> Velocity [m/s]
<b>Configuration 3 : 39 mm</b>		
Y-X		<ul style="list-style-type: none"> <li>0.002</li> <li>0.002</li> <li>0.002</li> <li>0.002</li> <li>0.001</li> <li>0.001</li> <li>0.001</li> <li>9.299e-04</li> <li>8.137e-04</li> <li>6.974e-04</li> <li>5.812e-04</li> <li>4.650e-04</li> <li>3.487e-04</li> <li>2.325e-04</li> <li>1.162e-04</li> <li>1.490e-08</li> </ul> Velocity [m/s]
Z-X		<ul style="list-style-type: none"> <li>0.002</li> <li>0.002</li> <li>0.002</li> <li>0.002</li> <li>0.001</li> <li>0.001</li> <li>0.001</li> <li>9.299e-04</li> <li>8.137e-04</li> <li>6.974e-04</li> <li>5.812e-04</li> <li>4.650e-04</li> <li>3.487e-04</li> <li>2.325e-04</li> <li>1.162e-04</li> <li>1.490e-08</li> </ul> Velocity [m/s]

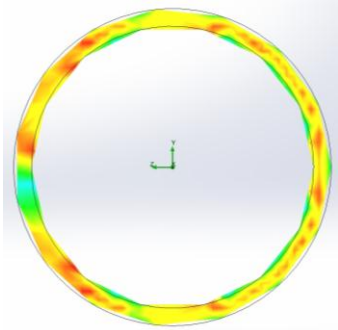
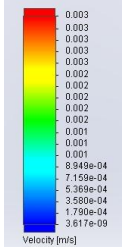
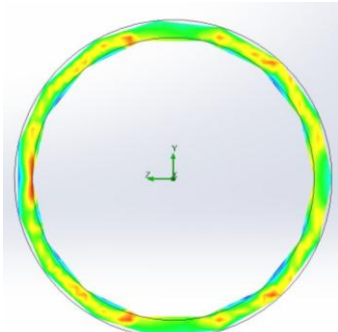
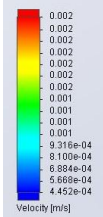
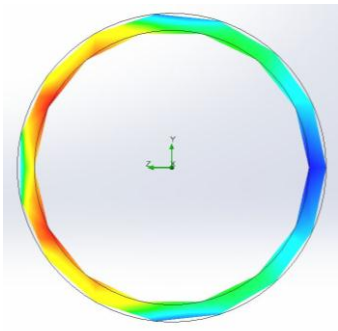
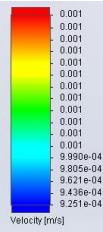
Naturally, when the solution enters the spinneret annulus; the velocity increases and initially appears irregular. As the solution travels down the annulus, the flow develops steadier regular flow. Longer residence time of the solution allows the solution to develop steady and lower velocity compared to shorter residence time. Table 4 shows velocity gradient inside the annulus for the three combinations. Shorter annulus in combination 1: Plane Z-X shows that the flow appears irregular and faster towards the end of the annulus compared to combination 3. This might explain why agglomeration occurs in combination 1 spinning. Table 5 shows the maximum and minimum velocity recorded for each combination. It shows that the max velocity recorded in configuration 3 is slower at  $1.66 \times 10^{-3}$  m/s compared to configuration 1, which is at  $4.451 \times 10^{-3}$  m/s. There is different velocity behavior between Y-X Plot and Z-X Plot. In Y-X Plot, the velocity gradient appears almost symmetrical where unsteady velocity occurs at the inlet section of the annulus before it stabilizes. In Z-X Plot, the velocity gradient is not symmetry and appears unsteady in the top quadrant all the way to the end of the annulus. By considering the quadrant involve and the solution inlet position, which is located at the side of the spinneret (top quadrant). We deduced that the solution is forced to travel faster and unstable at the top quadrant due to the shorter distance it needs to travel. Compared to the bottom quadrant, the solution travels longer before entering the annulus.

**Table 5. Velocity Range.**

<b>Configuration</b>	<b>Plane</b>	<b>Min. Velocity (m/s x 10<sup>-8</sup>)</b>	<b>Max. Velocity (m/s x 10<sup>-3</sup>)</b>
1: 29 mm	Y-X	1.7496	4.4510
	Z-X	0.3616	3.2210
2: 34 mm	Y-X	2.1626	2.8539
	Z-X	0.2205	2.2558
3: 39 mm	Y-X	4.1802	1.6600
	Z-X	1.4897	1.8590

The difference in velocity at the exit of the annulus might contribute to eccentricity problem as observed in the spun hollow fiber membrane. To put this statement into perspective, another cut plot at the annulus exit is generated as shown in Table 6. The velocity gradient shows that higher velocity is observed on the left side of the annulus (top quadrant) compared to the right side. The high velocity solution when travels down the channel will give more kinetic energy up to a maximum value at the tip of the channel. Due to the irregularity velocity at the outlet of the annulus, it will cause; a) Undesirable flow induced vibration at the channel, b) The solution exiting the annulus is irregularly unstable due to asymmetry velocity gradient. These phenomena will cause un-even thickness and structural damage of the spun hollow fiber membrane. The exit surface data also shows that the average velocity is lower at 0.001 m/s for combination 3 compared to 0.003 m/s for combination 1 further sustenance previous argument.

**Table 6. Velocity Gradient Near Annulus Exit.**

Velocity Gradient	Scale	Exit Data
<b>Configuration 1: 29 mm</b>		
		Min. Velocity (m/s)
		$2.616 \times 10^{-5}$
		Max. Velocity (m/s)
		0.007
		Ave. Velocity (m/s)
0.003		
<b>Configuration 2: 34 mm</b>		
		Min. Velocity (m/s)
		$8.594 \times 10^{-6}$
		Max. Velocity (m/s)
		0.003
		Ave. Velocity (m/s)
0.002		
<b>Configuration 3: 39 mm</b>		
		Min. Velocity (m/s)
		$8.905 \times 10^{-6}$
		Max. Velocity (m/s)
		0.002
		Ave. Velocity (m/s)
0.001		

## CONCLUSIONS

Three spinnerets with different nozzle's length have been fabricated in this project. Spinning of hollow fiber membrane were done using these three nozzles and the spun membrane were observed under SEM for its morphology. Computational simulation was completed as a supplementary initiative to rationalize the observed morphology:

- a. Inspection of scanning electron microscope figure shows that hollow fiber membrane produced using combination 3: 39 mm is symmetrically more pronounced and better structural integrity compared to combination 2: 34 mm. This is probably due to the flow in 39 mm is a stable steady flow.
- b. Longer residence time of the dope solution inside the channel gives a better chance for the solution flow to become steady, contributing to better hollow fiber membrane morphology.
- c. The symmetrical degree of flow velocity (at the annulus outlet) helps to determine morphology of the spun hollow fiber membrane. An irregular velocity gradient at the annulus exit introduces vibration and uneven extrusion of the solution. Thus, affecting the spun hollow fiber membrane structure.
- d. To improve the morphology of the hollow fiber membrane, the following suggestions are recommended;
  - i. Longer annulus is highly preferred; this will allow higher residence time of the dope solution inside the annulus allowing it to develop a steady flow before exiting the spinneret.
  - ii. Design of the spinneret need to account for solution trajectory; designers need to ensure that symmetrical flow is achieved when the solution enters the annulus minimizing the effect of irregular flow inside the annulus.

## ACKNOWLEDGEMENT

The authors would like to thank MOSTI for funding this research project and SKTM UMS for providing research lab to conduct the related experiment. We are also would like to extend our gratitude to Membrane Research Group members especially Ms. Zykamila Kamin for their constructive help and suggestions on this work.

## REFERENCES

- Bird, R. B., Armstrong, R. C., & Hassager, O. 1987. *Dynamics of Polymeric Liquids Fluid Mechanics*. Vol. 1, 2<sup>nd</sup> ed., John Wiley and Sons.
- Bonyadi, S., & Chung, T. S. 2007. Investigation of Corrugation Phenomenon in the Inner Contour of Hollow Fibers during the Non-solvent Induced Phase-separation Process, *Journal of Membrane Science*, **299**: 200.
- Chung, T. S., Teoh, S. K., Lau, W. W. Y., & Srinivasan, M. P. 1998. Effect of Shear Stress within the Spinneret on Hollow Fiber Membrane Morphology and Separation Performance. *Industrial & Engineering Chemistry Research*, **37**: 3930.
- Chung, T. S., Qin, J. J., & Gu, J. 2001. Effect of Shear Rate within the Spinneret on Morphology, Separation Performance and Mechanical Properties of Ultrafiltration Polyethersulfone Hollow Fiber Membranes. *Chemical Engineering Science*, **56**: 5869.
- John F. D., Janusz M. G., & John A. S. 2001. *Fluid Mechanics*. Essex, England: Pearson Education Limited.

- Larson, R. G. 1992. Instabilities in Viscoelastic Flows. *Rheologica Acta*, **31**: 213
- Li, K. 2007. *Ceramic Membrane for Separation and Reaction*. West Sussex, England: John Wiley and Sons Ltd.
- Moynihan, R. H., Baird, D. G., & Ramanathan. 1990. Additional Observations on the Surface Melt Fracture Behavior of Linear Low-density Polyethylene. *Journal of Non-Newtonian Fluid Mechanics*, **34**: 255.
- Nunes, S. P., & Peineman, K. 2006. *Membrane Technology in the Chemical Industry*. Wiley-VCH.
- Nijdam, W., de Jong, J., van Rijn, C. J. M., Visser, L. Versteeg, Kapantaidakis, G., Koops, H., & Wessling, M. 2005. High Performance Micro-engineered Hollow Fiber Membranes by Smart Spinneret Design. *Journal of Membrane Science*, **256**: 209.
- Otter, J. L. 1971. Some Investigations of Melt Fracture, *Rheologica Acta*, **10**: 200.
- Petrie, C. J. S., & Denn, M. M. 1976. Instabilities in Polymer Processing. *AIChE Journal*, **22**: 209.
- Porter, M. C. 1990. *Handbook of Industrial Membrane Technology*. New Jersey, USA: Noyes.
- Piau, J. M., Kissi, N. E., & Tremblay, B. 1990. Influence of Upstream Instabilities and Wall Slip on Melt Fracture and Sharkskin Phenomena during Silicones Extrusion through Orifice Dies. *Journal of Non-Newtonian Fluid Mechanics*, **34**.
- Piau, J. M., Kissi, N. E., & Tremblay, B. 1988. Low Reynolds Number Flow Visualization of Linear and Branched Silicones Upstream of Orifice Dies. *Journal of Non-Newtonian Fluid Mechanics*, **30** :197.
- Qin, J. J., Gu, J., & Chung, T. S. 2001. Effect of Wet and Wet-jet Spinning on the Shear-induced Orientation during the Formation of Ultrafiltration Hollow Fiber Membranes. *Journal of Membrane Science*.
- Santoso, Y. E., Chung, T. S., Wang, K. Y., & Weber, M. 2006. The Investigation of Irregular Inner-Skin Morphology of Hollow Fiber Membranes at High Speed Spinning and the Solutions to Overcome It. *Journal of Membrane Science*, **182**: 57.
- Su, Y., Lipscomb, G. G., Balasubramaniam, H., & Lloyd, D. R. 2006. Observations of Recirculation in the Bore Fluid During Hollow Fiber Spinning, *AIChE Journal*, **52**: 2072-2078.
- Su, Y. 2007. *Theoretical Studies of Hollow Fiber Spinning*. Ph. D. Diss., College of Engineering, University of Toledo.
- Wang, K. Y., Matsuura, T., Chung, T. S., & Guo, W. F. 2004. The Effects of Flow Angle and Shear Rate within the Spinneret on the Separation Performance of Poly (Ethersulfone) (PES) Ultrafiltration Hollow Fiber Membranes. *Journal of Membrane Science*, **240**: 67.
- Widjojo, N., & Chung, T. S. 2006. The Thickness and Air-gap Dependence of Macrovoid Evolution in Phase-Inversion Asymmetric Hollow Fiber Membranes. *Industrial & Engineering Chemistry Research*, **45**: 7618.
- Widjojo, N., Chung, T. S., Arifin, D. Y., Weber, M., & Warzelhan, V. 2010. Elimination of Die Swell and Instability in Hollow Fiber Spinning Process of Hyperbranched Polyethersulfone (HPES) via Novel Spinneret Designs and Precise Spinning Conditions. *Chemical Engineering Journal*, **163**: 143-153.
- Yang, Q., Chung, T. S., Chen, S. B., & Weber, M. 2008. Pioneering Explorations of Rooting causes for Morphology and Performance Differences in Hollow Fiber Kidneydialysis Membranes Spun from Linear and Hyperbranched Polyethersulfone. *Journal of Membrane Science*, **313**: 190.
- Yang, Q., Chung, T. S., Weber, M., & Wollny, K. 2009. Rheological Investigations of Linear and Hyperbranched Polyethersulfone Towards Their As-spun Phase Inversion Membranes' Differences. *Polymer*, **50**: 524.